In-and out-plane transport properties of chemical vapor deposited TiO 2 anatase films

Adeline Miquelot, Laurène Youssef, Christina Villeneuve-Faure, N Prud'Homme, N Dragoe, A Nada, Vincent R. Rouessac, S Roualdes, J Bassil, M Zakhour, et al.

Journal of Materials Science, 2021, 56, 10458–10476

In- and out-plane transport properties of chemical vapor deposited TiO_2 anatase films

A. Miquelot[1], L. Youssef[2,3], C. Villeneuve-Faure[4*], N. Prud'homme[5], N. Dragoe[5], A. Nada[2,6], V. Rouessac[2], S. Roualdes[2], J. Bassil[3], M. Zakhour[3], M. Nakhl[3], C. Vahlas[1]

[1]CIRIMAT, Université de Toulouse, CNRS, INPT, Toulouse, France

[2]Institut Européen des Membranes, IEM UMR 5635, Univ Montpellier, ENSCM, CNRS, Montpellier, France

[3]LCPM/PR2N, Lebanese University, Beirut, Lebanon

[4]LAPLACE, Université de Toulouse, CNRS, INPT, UPS, Toulouse, France

[5]ICMMO, Université Paris Sud, Université Paris-Saclay, Orsay, France

[6]Dept. of Analysis and Evaluation, Egyptian Petroleum Research Institute, Cairo, Nasr City, P.B. 11727, Egypt

[*] Corresponding author christina.villeneuve@laplace.univ-tlse.fr

Keywords: TiO_2, thin film, transport properties, C-AFM, MOCVD, PECVD

ABSTRACT

Due to their polymorphism, TiO_2 films are quintessential components of state-of-the-art functional materials and devices for various applications from Dynamic Random Access Memory to Solar Water Splitting. However, contrary to other semiconductor/dielectric materials, the relationship between structural/morphological and electrical properties at the nano and micro scales remains unclear. In this context, the morphological characteristics of TiO_2 films obtained by Metal-Organic Chemical Vapor Deposition (MOCVD) and Plasma Enhanced Chemical Vapor Deposition (PECVD), the latter including nitrogen doping, are investigated and they are linked to their in-plane and out-plane electrical properties. A transition from dense to tree-like columnar morphology is observed for the MOCVD films with increasing deposition temperature. It results in the decrease of grain size and the increase of porosity and disorder, and subsequently it leads to the decrease of lateral carrier mobility. The increase of nitrogen amount in the PECVD films enhances the disorder in their pillar-like columnar

morphology along with a slight increase of density. A similar behavior is observed for the out-plane current between the low temperature MOCVD films and the undoped PECVD ones. The pillar-like structure of the latter presents a lower in-plane resistivity than the low temperature MOCVD films, whereas the out-plane resistivity is lower. The tree-like columnar structure exhibits poor in- and out-plane conductivity properties whereas pillar-like and dense TiO_2 exhibit similar in- and out-plane conductivities even if their morphologies are noticeably different.

Graphical abstract

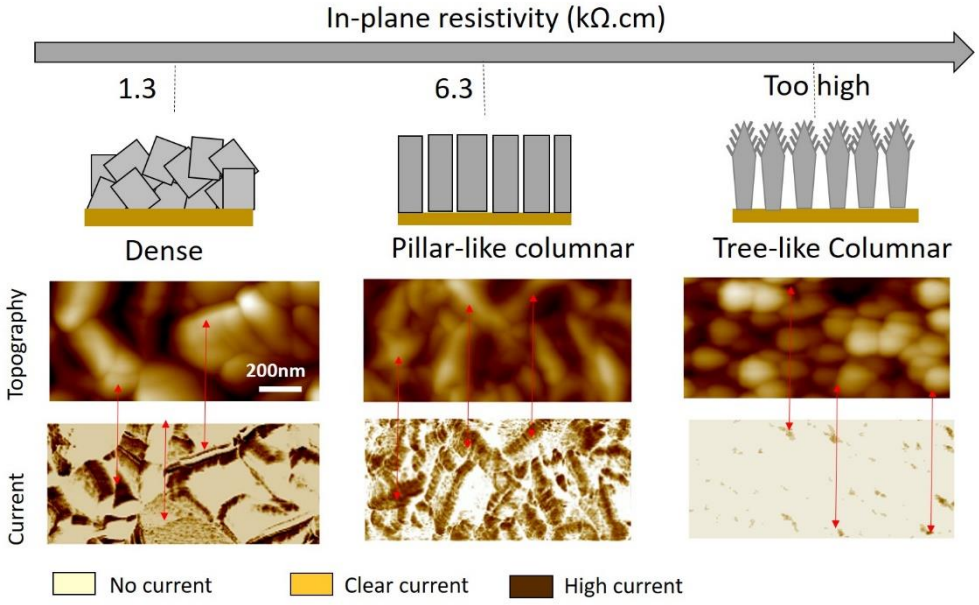

Introduction

TiO_2-based thin films have been probably the most investigated inorganic material during the past decades, due to their promising properties in numerous applications such as Dynamic Random Access Memory [1] (DRAM), photovoltaic [2] (PV) or solar water splitting [3-4] (SWS) devices. Despite the wealth of data on this material, monitoring and optimization of the properties of TiO_2 films are still required. Indeed, TiO_2 film morphology strongly impacts electrical properties and more particularly charge transport [5] which, in turn conditions the performance of devices in above-mentioned applications.

In the literature, TiO_2 films have been obtained by various techniques such as physical vapor deposition [6] (PVD), atomic layer deposition (ALD) [7], metalorganic or plasma enhanced chemical vapor deposition (MOCVD, PECVD) [8-11], reactive magnetron sputtering [12] and liquid techniques such as sol-gel [13] or electrodeposition [14]. This large variety of techniques results in a wealth of morphological forms and crystalline phases. Concerning anatase TiO_2 thin films, numerous studies demonstrated a broad resistivity range (from 10^{10} Ω cm to 10 Ω cm [15-18]), in strong correlation with crystalline phases and/or morphology [15-16, 19-23].

Considering SWS application, the anatase TiO_2 columnar morphology results in an increased specific surface area which is deleterious to the barrier properties [24] and inversely, is favorable to the (photo-)catalytic properties of the TiO_2 films [25]. However, Pilkington tests demonstrate a degradation rate of 10% [26] and 90% [27] after 180 min, for columnar TiO_2 films processed by PECVD and MOCVD respectively. Moreover, N-doping is required for columnar PECVD films to reach the same degradation rate (verifier s'il s'agit de "amount" ou de "rate") as columnar MOCVD ones. Consequently, the morphology does not entirely explain these differences and electrical properties need to be probed in relation to morphology, at the nanoscale. Some attempts have been done to determine the relationship between electrical properties and morphology. For example, it has been shown that, in a microstructure composed of small TiO_2 nanorods, carriers exhibit lower mobility than in large crystallites [28]. Moreover, interestingly, Murakami *et al*. have investigated out-plane electrical properties combining macroscale current-voltage characteristics and conductive atomic force microscopy (C-AFM) mapping to show that conduction occurs through grains and that current magnitude depends on the precursor nature for ALD processed rutile-TiO_2/RuO_2 stacks [29].

In this context, the objective of this paper is to identify the interplay between the morphology of TiO_2 films and the in- and out-plane electrical properties for SWS application. We present a comparison between in-plane electrical properties such as resistivity or carrier mobility and out-plane current paths at nanoscale while considering various morphologies. To reach this goal, we focus on TiO_2 anatase films with different morphologies (from dense to columnar), broad conductivity range and involvement in different applications (PV, SWS…). Among all the available techniques, we use two different deposition techniques, namely PECVD and MOCVD, to obtain TiO_2 films with different structure, morphologies and photoelectrochemical properties [26-27]. This choice is based on the fact that both techniques yield films of a characteristic columnar morphology that can be monitored by varying the deposition temperature [26, 30] and/or the N-doping ([22, 27]) of the films, as envisaged in this study. Another reason for investigating the N-doping approach lies in the influence of N-doping on the conductivity (disorder, traps, states close to conduction band, etc. [31]) and in the introduction of recombination centers favorable to photo-catalytic activity under solar activation. It is worth noting that the two CVD techniques yield engineering materials of high structural and morphological complexity, in contrast with those obtained by magnetron sputtering, for example. The latter can serve to create one to one correlations between particular structural and functional characteristics that could feed ad hoc libraries, useful in a material by design approach. Nonetheless, the extent of such correlations is far beyond the contours of a sole publication. In addition, the adopted CVD processes are scalable, easily tunable in terms of support geometry and the identified correlations, although tentative, can be readily available for fast technological implementations. In this perspective, we combine Van der Pauw, Hall effect and C-AFM methods to investigate the in- and out-plane electrical properties. We confront them to the structural and morphological characteristics of the films and we thus establish trends in the interplay between process, morphology and electrical properties of the films.

In our previous studies [26-27], we highlighted morphological and structural characteristics of the PECVD and MOCVD films of interest. Table 1 summarizes the obtained results, which are key parameters to be correlated with the electrical properties at micro- and nanoscales investigated in this study. The electrical properties of with columnar (pillar-like or tree-like) morphologies are expected to present significant differences out-plane (i.e. along columnar grain) and in-plane (i.e. between grains) directions. Consequently, we proceed to a systematic investigation of in both directions with the aim to reveal the interplay between electrical

properties and morphology in such anisotropic structures. Since dense TiO_2 films present a more isotropic structure, in- and out-plane electrical properties should display the same behavior.

Table 1 Morphological and structural properties of MOCVD- and PECVD-processed films.

	MOCVD-processed films [26]	PECVD-processed films [27]
Crystalline form	Fully crystallized pure anatase structure (whatever Td*)	Pure anatase structure: fully crystallized (if non-doped) or partially amorphous (if doped)
Crystallographic orientations	Mostly <100> oriented (at low Td*) to mostly <110> oriented (at high Td*) structure	Mostly <101> oriented structure (whatever doped or non-doped)
Nanoscale morphology	From dense (at low Td*) to tree-like columnar (at high Td*) morphology. As a consequence: increasing porosity and disorder with Td*	Pillar-like micro-columnar morphology: from ordered (if non-doped) to disordered (if highly doped)

*Td: deposition temperature

Materials and Methods

Sample processing

TiO_2 films with thickness in the 100-400 nm range were obtained from titanium tetraisopropoxide (TTIP > 97 %, Sigma-Aldrich). MOCVD was performed in a vertical, cylindrical, stagnant flow cold wall stainless steel reactor previously described in detail [32]. TTIP was conditioned in a glass bubbler maintained at 20.5 °C and N_2 was used as both carrier and dilution gases. Their respective partial pressure was 0.35 Pa for the TTIP (calculated from the estimated maximal TTIP flow from the empirical formula of Hersee *et al*. [33]), and 10.92 and 121.73 Pa for N_2. The total flow is 57 standard cubic centimeters per minute (sccm). All gas lines were thermally regulated at ca. 65 °C. Film deposition was performed on n-type doped Si wafers and fused silica plates at 133 Pa and temperatures ranging from 325 °C to 500 °C with various durations that were adapted to produce films of similar thickness of approximately 350 nm whatever the deposition temperature [26]. TiO_2 and N-doped TiO_2 films were equally deposited by a low frequency PECVD process according to a previously reported protocol [27]. The partial pressures of vapors and gases during the deposition were: 22.5 Pa for TTIP and Ar carrier gas, 17 Pa for O_2 oxidizing agent and 5 Pa or 15 Pa for NH_3 (added in the plasma reactor

for doping purpose in the case of N-TiO_2 films). The plasma discharge power was 64 W, the deposition time was 20 min and the deposition temperature was 350 °C for all the samples, in a one-step process. The films were deposited on p-type Si wafers and silica plates.

Morphological characterization

Films morphology was determined using Scanning Electron Microscopy, in secondary electron mode, on cross-section, on a S4800 Hitachi and a JEOL JSM 7600F instruments. Surface topography of the TiO_2 films was probed by AFM in tapping mode using Bruker multimode 8 setups, equipped with a Bruker Tespa-V2 silicon tip with a spring constant of 43.2 N m^{-1}. For each sample, the average surface roughness Ra was extracted on three different 5 × 5 μm^2 surface maps then yielded a mean value with a dispersion of *ca.* 5%.

Spectroscopic ellipsometry (SE) measurements were performed on a Semilab SE-2000 apparatus in the 170–1650 nm spectral range. A Cauchy optical model was used to describe the optical properties of the film and enabled to calculate films' thicknesses averaged on the analyzed area (an ellipse a × b = 10 × 3 mm^2) with a mathematical precision depending on the goodness of fit (GoF). The presented results have a minimum value of GoF equal to 0.98, which corresponds to a maximum uncertainty of ± 2 nm if GoF > 0.98. The ellipsometric porosimetry (EP) measurements were performed using a Semilab GES5E (250-1000 nm) instrument, completed with a lab-made closed chamber to control the surrounding vapor pressure of an intrusive probe for EP characterization. Before any EP measurement, the films deposited on silicon wafer were placed under vacuum (6.7 Pa) and the sample holder was heated at 200°C for 20 min in order to empty the pores from physisorbed contaminants, mainly water. Back to a room temperature, ethanol vapor was step by step introduced, each P/P_0 = 0.1, 0.2, etc. up to 1, where P is the ethanol partial pressure in the chamber and P_0 its saturating partial pressure at 25 °C. An ellipsometry measurement was performed at the end of each plateau (corresponding to a specific P/P_0 value). Isotherms of the ellipsometric parameters tan(Ψ) and cos(Δ) as a function of the ethanol pressure were collected using winSE/winElli softwares. Each measurement was modeled by an absorbent Cauchy model, which allows extracting the refractive index of the film as a function of the ethanol partial pressure. Its increase reflects the filling of the open pores with ethanol. By applying the Lorentz-Lorenz model on 3 phases (skeleton, ethanol and vacuum) on the value of the refractive index at 1.96 eV (633 nm), pore volume could be calculated. Using the Kelvin's law, the partial pressure of ethanol was converted into an estimated filled pore diameter. A maximal pore diameter of 20 nm can be analyzed with this setup, corresponding to a maximal ethanol partial pressure P/P_0 close to 0.89.

For MOCVD films, the total porosity was evaluated using a Lorentz-Lorenz anatase/air mix model. The band gap was evaluated using a Cody-Lorentz oscillator model.
The mass density of the PECVD films on Si wafer was determined by X-Ray Reflectrometry (XRR) using a Siemens/Bruker D5000 with a CuKα source (λ = 1.54056 Å). The error relative to the mass density is ± 0.05 g/cm^3.

Opto-electronic characterization

The film absorption in the 200-1650 nm range was measured by UV/Vis spectrophotometry, performed in reflection mode with a JASCO V-570 apparatus on the PECVD films deposited on Si wafer and in transmission mode using an Agilent-Cary 5000 apparatus on MOCVD films deposited on glass substrate. The band gap energy was calculated using the Tauc Plot method [34].

Carrier concentration was measured at room temperature using a laboratory made system in AC field [35]. The circuit was closed with Cu-Be pins on the films and measurements were made by applying a DC current with a Keithley 6221 source while oscillating a 1 T magnetic field at 1.4 Hz frequency. The Hall induced AC signal from films deposited on SiO_2 was measured with a Zurich Instrument MFLI lock in amplifier. With the instrument we measured samples below 0.1 V/(cm².s) [35] and several reports demonstrated that Hall effect in AC field was a viable route to the characterization of low mobility materials, down to a mobility range 0.001 V/(cm^2 s) [36-39].

Lateral electrical transport measurements were performed on films deposited on SiO_2 as well, in a laboratory made system composed of a Janis He-free cryostat CCS 200/204 coupled with a LabVIEW monitored Sumitomo SHI-APD 204 cryocooler. The measurements were made at room temperature under a vacuum below 1 Pa and dark configuration to avoid room light interference. The measurements in Van der Pauw mode were performed along the four Van der Pauw configurations by using a Keithley 6220 source coupled with a Pickering matrix card controlled by NI PXI 1075 mainframe. The voltage was measured by a Keithley 2182 nanovoltmeter while the applied current was measured with a Keysight 8193A PXI DMM instrument. The temperature was controlled within 50 mK by a Lakeshore 335 controller reading a Si-670 diode thermometer anchored on the cold finger of the cryostat. Eight measurements were performed for each temperature allowing the estimation of the related measurement error to be repeatable.

Transversal current measurements at nanoscale were performed with an AFM Bruker Multimode 8 setup equipped with a PtSi tip (curvature radius Rc = 27 nm and spring constant k = 1.7 N/m) using C-AFM mode. A DC voltage varying between 0 V and -8 V was applied on conductive silicon substrate and current was collected by PtSi tip. The measurements were performed owing to the 100 nA V^{-1} module sensitivity using a contact force of 27 nN. Current was probed over 2 × 0.5 μm^2 area at three different localizations of each sample, with good consistency. A 384 pixel-by-line was used for mapping, which implies a pixel size of 5.2 nm.

In order to evaluate the charge transfer resistance of the materials when immersed in an electrolyte solution, impedance measurements were performed in a previously described single compartment Teflon® cell [40]. A three electrodes configuration was used involving: the film deposited on a conductive support (E-Tek® carbon cloth for the PECVD films, n-type Si wafer for the MOCVD ones) as the anode (working electrode), a commercial glassy carbon material (0.7 cm × 2 cm) as the cathode (counter-electrode) and a commercial Ag/AgCl (3 M KCl) from SI Analytics® (0.197 V vs. RHE) as the reference electrode. The three electrodes were immersed in a 0.5 M H_2SO_4 liquid electrolyte solution prepared from a 100 % H_2SO_4 solution in 18 MΩ pure MilliQ® water (Merck Millipore). In order to ensure appropriate electron collection through the external circuit, both photo-anode and cathode were tightly connected to gold wires (≥ 99.9 %, GoodFellow) placed outside the electrolyte solution to avoid metallic interference. The experiments were performed in the dark by covering the whole cell with aluminum foil. Before each test, the oxygen dissolved in the electrolyte solution was eliminated by Ar bubbling for 40 min. Electrochemical Impedance Spectroscopy (EIS) was performed with a Solartron SI 1260 frequency analyzer in a range 0.02 Hz-10^5 Hz with 0 mV and 10 mV AC amplitude for the PECVD and MOCVD samples, respectively. ZPlot® and ZView® softwares (Scribner) were used to record and fit the experimental data. The charge transfer resistance was calculated by extrapolation of the curves to the real impedance axis with a circle fitting approach based on Nyquist diagram.

Results

TiO_2 morphological and structural properties: an overview

Table 2 resumes the thicknesses of the TiO_2 films, estimated by SE. The MOCVD films present quite the same thickness around 350 nm whereas the thickness of the PECVD films varies between 110 and 475 nm, depending on NH_3 pressure.

In previous studies (table 1), we demonstrated that whatever deposition technique, TiO_2 thin films are composed of pure anatase [41-42] in the investigated range of deposition parameters. MOCVD films are fully crystallized [26] whereas PECVD films also present an amorphous phase associated with doping [27].

Table 2 TiO_2 film thicknesses measured by SE on Si wafer

Process	Process parameter	Thickness (nm)
PECVD	0 Pa NH_3	475
	5 Pa NH_3	110
	15 Pa NH_3	230
MOCVD	325 °C	347
	350 °C	295
	375 °C	304
	400 °C	368
	450 °C	408
	500 °C	436

The cross sectional SEM micrographs of Fig. 1 allow comparing the morphologies of TiO_2 films processed by PECVD and MOCVD. A rod like shaped, columnar morphology is observed for films processed by PECVD in the absence of NH_3 (figure 1a). This morphology also prevails at high NH_3 pressure. Fig. 1b and 1c compares the in-depth morphology with the 25° tilted cross-sectional micrographs of MOCVD TiO_2 films processed at different temperatures. Their comparison reveals a morphological evolution from dense (325°C-350°C) to columnar (450°C-500°C), occurring between 375°C and 400°C [26]. Moreover, this transition is associated to a decrease in the size of the various structures. At high deposition temperature the columnar structure exhibits a sharp tree-like shape strongly different to the rod-like shape observed for PECVD films. Fig 1d schematically summarizes the related morphology of the different films.

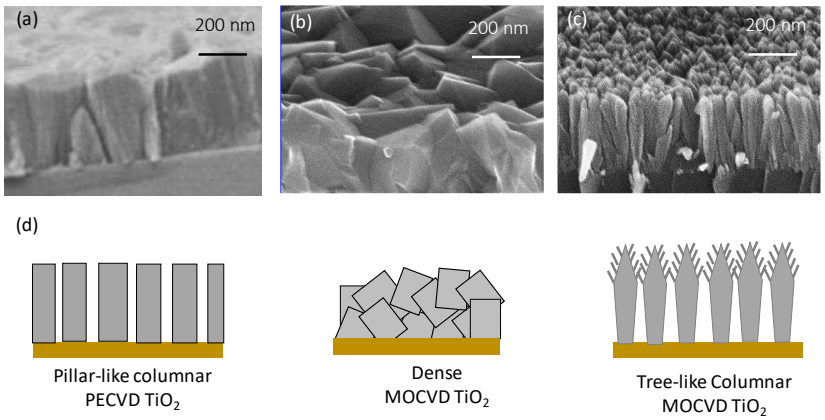

Figure 1 SEM micrographs of (a) PECVD films deposited at 0 Pa NH_3, and for MOCVD films deposited at (b) 325 °C and (c) 450 °C. Schematical illustration of the the observed morphologies (d).

Fig. 2 resumes the influence of the operating conditions for each process on the structure of the TiO_2 films. The increase of the NH_3 doping of the PECVD films results in a noticeable evolution of the surface morphology, illustrated in Fig. 2a and Fig. 2b by the decrease of grains lateral size from 100-200 nm for 0 Pa NH_3 to 10-20 nm for 15 Pa NH_3. The simultaneous decrease of the average value of R_a and slight increase of the density is observed (Fig.1f). A morphological evolution is also observed for the MOCVD films (Fig. 2c, 2d and 2e). The lateral dimensions of grain were determined from AFM picture. A transition from large grains at low temperature (100-200 nm at 325 °C) to small grains at high temperature (50 - 70 nm at 500°C). A transition takes place between 350 °C and 450 °C as observed in Fig. 2d with a mix of small and broad grains which is related to decrease of surface roughness and increase of the films porosity, illustrated in Fig. 1g. So porosity increasing could be related to the evolution of dense morphology obtained below 350 °C towards a tree-like (or dendritic) columnar one for higher temperatures, starting at 450 °C [26].

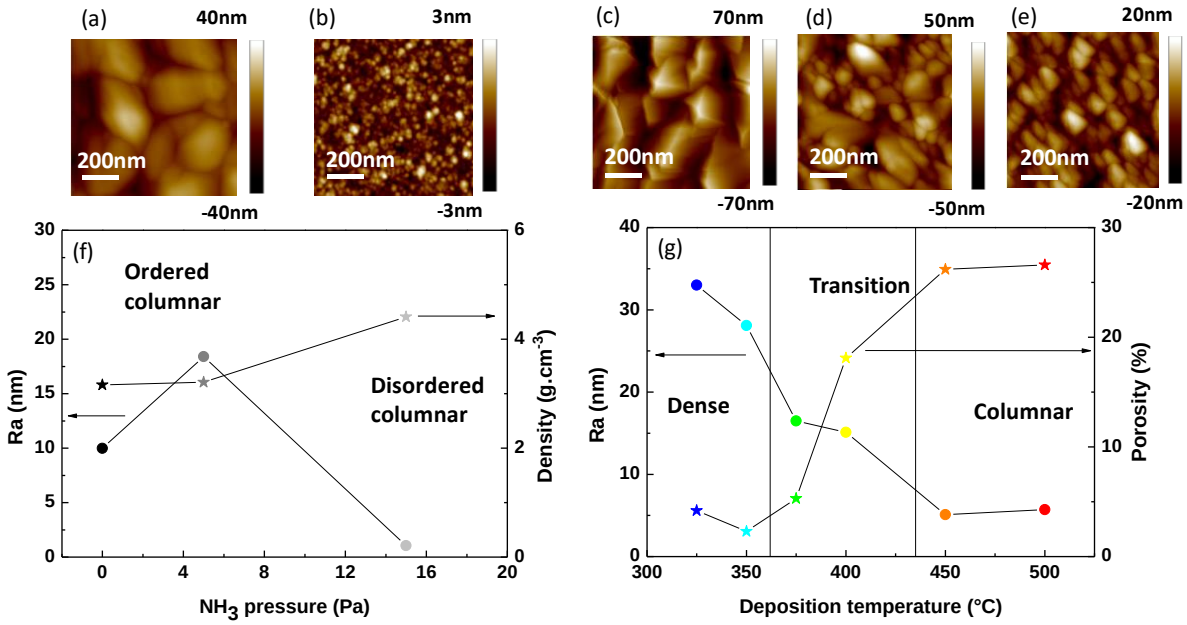

Figure 2 Surface topography probed by AFM on 1 × 1 μm² area for PECVD samples deposited at **a** 0 Pa and **b** 15 Pa NH_3, and for MOCVD ones deposited at **c** 325 °C, **d** 400 °C and **e** 500 °C. **f** Evolution, as a function of the NH_3 partial pressure, of the average surface roughness Ra over 5 × 5μm² and of the density for PECVD films. In this, and the forthcoming diagrams of the PECVD films, black, grey and light grey color code corresponds to NH_3 pressure of 0, 5 and 15 Pa. **g** Evolution, as a function of the deposition temperature, of the average surface roughness Ra over 5 × 5μm² and of the mesoporosity for MOCVD films. In this, and the forthcoming diagrams of the MOCVD films, the dark blue, light blue, green, yellow, orange, and red color code corresponds to deposition temperatures of 325, 350, 375, 400, 450, and 500 °C, respectively.

These results demonstrate that the two techniques yield TiO_2 film structures with different morphologies, leading to various roughness and porosity values, which are expected to influence the electrical properties at micro- and nanoscales as it will be shown in the next part. Fig. 3 presents the evolution of the band gap E_g, obtained from UV-vis absorption spectra using the Tauc-plot method, as a function of the NH_3 pressure and the deposition temperature for the PECVD and the MOCVD films, respectively. The related transmission spectrum and Tauc plots, used to extract E_g, are reported in annex 2 (Fig. A2). A strong gap narrowing is observed with increasing NH_3 pressure, which is attributed to the incorporation of nitrogen atoms in the atomic organization structure [41-42], acting as donors. A slight increase of Eg with the deposition temperature is observed for the MOCVD films. This may be due to various parameters such as an increase of oxygen vacancies, of porosity (surface defects) or of the disorder in the structure [43-44]. However, the E_g values, and therefore their evolution with the temperature increase, are questionable, due to scattering and interference fringes that decrease the reliability of the Tauc plot method [26].

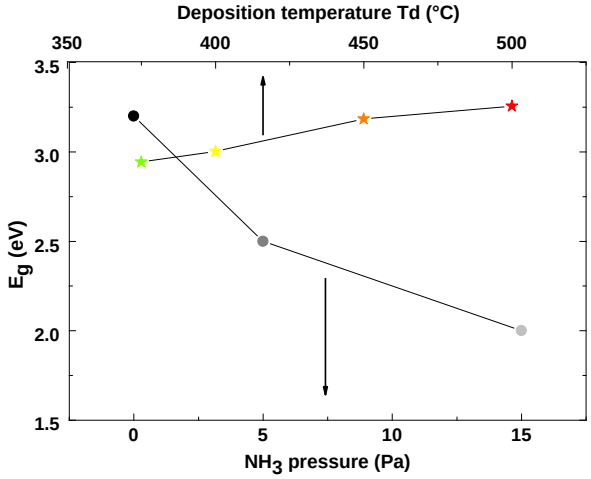

Figure 3 Evolution of energy band gap E_g determined by UV-visible spectroscopy as a function of NH_3 partial pressure for PECVD (circles) and deposition temperature (stars) for MOCVD TiO_2 films.

Lateral transport in TiO_2 films: a microscale study First, the lateral electrical properties of TiO_2 were determined at the microscale in Van der Pauw geometry (electrodes deposited over the surface). These measurements were performed on TiO_2 films deposited on SiO_2 substrate. In the literature, few studies have demonstrated that substrate has a strong influence of films morphology and related electrical properties [45-46]. However, XRD patterns (annex 1 Fig. A1) demonstrate no substrate influence on films crystallographic structure. Consequently, electrical properties could be investigated for films deposited on SiO_2 and transposed to ones deposited over Si.

For the MOCVD films deposited at 325, 350 and 375 °C the current versus voltage characteristic was acquired at room temperature. These characteristics present a linear behavior

associated to only weak asymmetry. Thus, electrical contacts exhibit a Schottky-type barrier [47] allowing the estimation of the lateral resistivity ρ of these samples. Moreover, the high lateral electrical resistivity of the MOCVD films processed at high temperatures (i.e. 400, 450 and 500 °C) prevents the determination of the current versus voltage characteristics, possibly due to the tree-like columnar structure with high porosity between grains.

The values of ρ, at room temperature of the MOCVD samples were summarized in Table 3. We note an increase in the lateral electrical resistivity with the deposition temperature, which is consistent with the band gap values. Comparing these results to those reported in the literature is quite hazardous because a lot of parameters are influent (deposition techniques, deposition conditions, substrate…). So, few pertinent results are reported in the Table 4 for comparison. First of all, it is important to notice a strong dispersion on resistivity values. Our values are similar to those obtained for sol-gel deposited films [16, 48] or Reactive DC sputtering over glass substrate [46] and lower than those processed by MOCVD [49].

Table 3 Lateral resistivity at 293 K and carrier concentrations of MOCVD and non-doped PECVD films.

Deposition process	**Process parameter**	**Lateral resistivity ρ (Ω. cm)**	**Carriers concentration n (×10^{18} cm^{-3})**	**Mobility μ (cm^2 V^{-1} s^{-1})**
PECVD	0 Pa	$6.7\times10^3 \pm 4\times10^2$	$1.8\times10^{-2} \pm 1\times10^{-3}$	$5.2\times10^{-2}\pm6\times10^{-3}$
MOCVD	325°C	$1.3\times10^3 \pm 4$	1.0 ± 0.3	$6\times10^{-3} \pm 2\times10^{-3}$
	350°C	$2.1\times10^3 \pm 1\times10^2$	-	-
	375°C	$1.1\times10^5 \pm 1\times10^3$	-	-
	400°C	Out of range	2.9 ± 0.2	-
	500°C	Out of range	-	-

Table 4 Electrical properties of anatase TiO_2 films as reported in the literature.

Deposition technique	**Substrate**	**Deposition conditions**	**Measurement configuration**	**Electrical properties**
MOCVD [49]	LAST (100)	TDMAT 600°C	Lateral (Hall electrodes)	$\rho = 2.1\times10^6$ Ω. cm $n = 1\times10^{18}$ cm^{-3}
Sol gel [16]	Si	300°C-700°C	Lateral (four probes)	$\rho = 1.4\times10^4$ Ω. cm (300°C) $\rho = 0.2\times10^4$ Ω. cm (700°C)
Reactive triode sputtering [15]	-	300°C – 400°C	Lateral (Van der Pauw)	$\rho \approx 8\times10^{-2}$ Ω. cm
DC reactive sputtering [46]	Glass	-	-	$\rho = 5.5\times10^3$ Ω. cm
	Si	-	-	ρ = 2-5 Ω. cm

The carrier concentration *n* was measured by Hall Effect for the MOCVD samples and reliable values were obtained for those deposited at 325 and 400 °C (Table 3). Despite the high

resistivity of the sample synthetized at 400°C, we succeeded in measuring the carrier concentration by Hall Effect in AC set up. Indeed, the two methods of measurements are totally different. Resistivity measurements by Van der Pauw requires eight successive measurements and are sensitive to small thermal fluctuations. The Hall effect measurements are performed at a fixed AC frequency with a lock-in amplifier which makes the measures insensitive to thermal variations. The values are in the same range of ca. 10^{18} cm^{-3} which is comparable of those obtained by Wang et al. [49] and are one order of magnitude lower than values reported in the literature [50]. As TiO_2 is an n-type semiconductor, we assume one type of majority carrier (electron in this case). The resulting carrier mobility μ could be deduced using the following equation:

$$\mu = \frac{1}{\rho \times n \times e} \quad (1)$$

with e the absolute value of electron charge (1.6 10^{-19} C).

For the sample deposited at 325 °C (the only one for which it was possible to measure both lateral resistivity and carrier concentration) an electron mobility of $4.8 \pm 2 \times 10^{-3}$ cm^2 V^{-1} s^{-1} was determined. Moreover, as the carrier concentration remains in the same order of magnitude with increasing the deposition temperature, together with a marked increase in the lateral resistivity, we assume that the carrier mobility decreases with the deposition temperature. This carrier mobility decrease could be related to various parameters such as transition from dense to columnar microstructure (i.e. from isotropic to anisotropic structure), an increase in the defects concentration and/or decrease of the grains size [20, 22].

Van der Pauw and Hall effect measurements failed on doped PECVD films, which could be attributed to their high lateral resistivity. Current versus voltage investigation in Van der Pauw configuration of the undoped PECVD film results in a linear behavior. The obtained value of the lateral resistivity ρ at room temperature is 6700 Ω cm. The measured values of carrier concentration extracted from Hall effect measurements and of carrier mobility for this sample are reported in table 3. The values of ρ for the undoped PECVD and the low temperature MOCVD films are comparable, whereas the carrier concentration of the former one is two orders of magnitude smaller. This implies that the PECVD films present better carrier mobility than the MOCVD ones. This behavior could be related to complex contribution of the carbon impurities in PECVD films [51] which can act as carriers and/or defects in the film.

Transversal transport in TiO_2 films: a nanoscale study

Fig. 4 compares C-AFM results for PECVD films obtained at various NH_3 pressures. Simultaneous consideration of morphology (Fig. 4a) and corresponding current map (Fig. 4b) of the undoped film reveals that the current flows through some facets (see arrows on Fig. 4a and 4b). The occurrence diagram depicted on Fig. 4c represents the statistical distribution of current values over the surface. The dark grey area under the curve refers to the conductive area, determined between fixed boundaries. It reveals that the conductive area ranging from -5 nA to -250 nA for an applied bias voltage of -3 V, represents a broad dispersion of approximately over 92 % of the total surface.

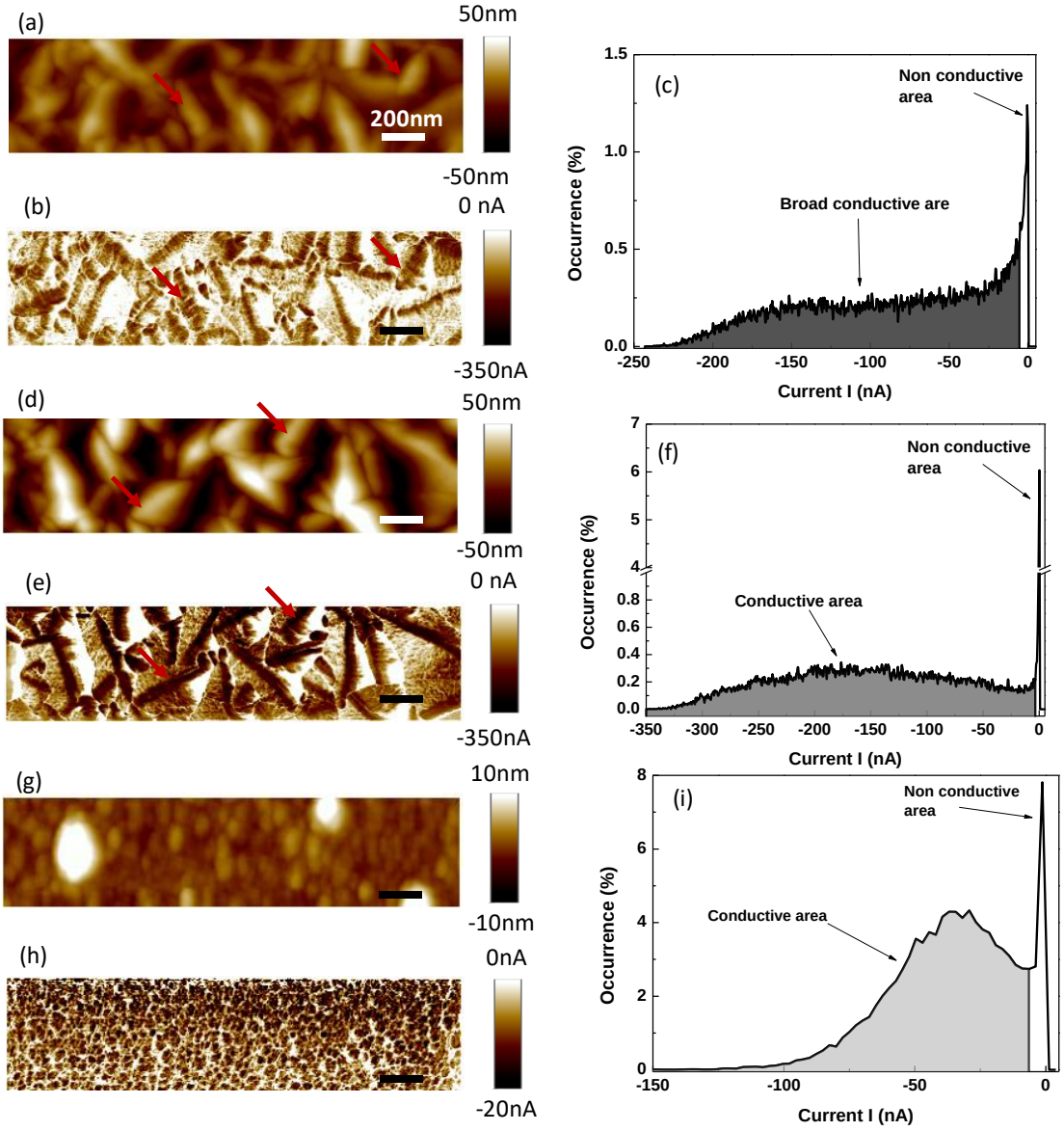

Figure 4 a Topography and **b** current maps, and **c** corresponding occurrence diagrams obtained with bias voltage of -3 V for the undoped PECVD film. **d** Topography and **e** current maps, and **f** corresponding occurrence diagram obtained with bias voltage of -3 V on PECVD films processed at 5 Pa NH_3 partial pressure. **g** Topography and **h** current maps, and **i** corresponding occurrence diagram obtained with an applied bias voltage of -3 V on PECVD films processed at 15 Pa NH_3 partial pressure.

Scale bar corresponds to 200 nm for each AFM micrographs and red arrow correspond to conductive grain facets for TiO_2 films, undoped and processed at 5 Pa NH_3.

Simultaneous consideration of morphology (Fig. 4d) and corresponding current C-AFM maps (Fig. 4e) for low-doped films (i.e. 5 Pa NH_3) reveals that, as for undoped films, the current flows through some facets. The occurrence diagram of Fig. 3f shows that the amount of conductive (grey) area, ranging from -5 nA to -350 nA for an applied bias voltage of -3 V, represents 86 % of surface, which also represents a broad dispersion. For higher nitrogen amount (i.e. 15 Pa NH_3), the behavior is quite different. Indeed, simultaneous consideration of morphology (Fig. 3g) and corresponding current maps (Fig. 4h) shows that the current flows through the entire grains. Moreover, the occurrence diagram shows that the amount of conductive area (light grey area on Fig. 4i) represents 85 % of surface ranging from -2 nA to -120 nA for an applied bias voltage of -3 V, which represents a lower dispersion than in the undoped and low-doped films.

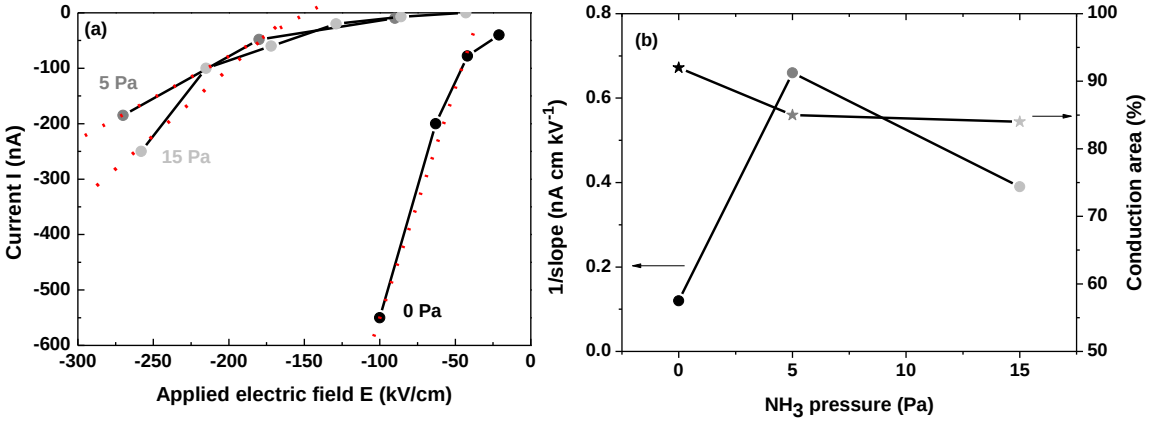

Figure 5 a C-AFM current versus applied electric field curves, probed in conductive area (facets or entire grains) for TiO_2 films processed by PECVD at different NH_3 partial pressures. Linear part of current versus electric field is depicted in red dot to extract slope. **b** evolution of the inverse of slope and conduction area as function of NH_3 pressure.

To compare these films exhibiting different thicknesses, Fig. 5a presents the evolution of the current as a function of the electric field. The current is probed on conductive area, which corresponds to the mean value on occurrence diagrams (Fig. 4c, 4f and 4i). The undoped sample presents the conductive area with the highest conduction level, compared to the 5 Pa and 15 Pa-doped samples, which present comparable current versus electric field curves whereas conduction occurred at different localization (facets vs entire grains). These are not linear which

implies the existence of a Schottky barrier at the interface between PtSi electrode and TiO_2 films. Due to the inhomogeneous distribution of the electric field induced by tip-plane configuration, barrier height or resistivity is not possible. However, the slope of the characteristics is related to the conductivity. From Fig. 5a the slope of the linear part is extracted (red dots), which reflects in first approximation the behavior of the inverse of transversal resistance. Fig. 5b represents the evolution of the inverse of slope and of the conduction area as function of NH_3 partial pressure. An increasing of pressure induces an increasing of transversal electrical resistance along columnar grain. This increasing is accompanied by a low decreasing of conduction area, which implies an increasing of transverse resistance at microscale.

Fig. 6 compare C-AFM results for TiO_2 films deposited by MOCVD at 325 °C (dense morphology) and 400 °C (transition morphology) for an applied bias voltage of -3 V. Comparison of surface morphology (Fig.6a) and current map (Fig.6b) for films processed at 325 °C shows that conductive areas correspond to facets (see arrow for localization). The occurrence diagram (Fig.6c) emphasizes three different areas. (i) A non-conductive area, which represents 45 % of the total surface. (ii) A low conduction area (labelled Area A1), which amount represents around 53% of the total surface. This presents a broad dispersion ranging from -2 nA to -200 nA for an applied bias voltage of -3 V. (iii) A high conduction area (labelled Area A2), which represents around 3% of the total surface. This presents a weak dispersion ranging from -545 nA to -552 nA for an applied bias voltage of -3 V.

A rather similar phenomenon occurs for films processed at 400°C. Indeed, the comparison of surface morphology (Fig. 6d) and current map (Fig. 6e) shows that conductive areas correspond to facets. The occurrence diagram (Fig. 6f) emphasizes three different areas. (i) A non-conductive area, which represents 55 % of the total surface. (ii) A low conduction area (labelled Area A1), which amount represents around 43 % of the total surface. This presents a broad dispersion ranging from -200 pA to -1.25 nA for an applied bias voltage of -3 V. (iii) A high conduction area (labelled Area A2), which represents around 2 % of the total surface. This presents a broad dispersion ranging from -1.25 nA to -3 nA for an applied bias voltage of -3 V.

High applied bias voltage is needed to probe an ultra-low current flowing through facets in films processed at temperature higher than 400 °C. Indeed, for an applied bias voltage of -7 V, 95 % of the surface is non-conductive and current values as low as -200 pA and -70 pA are reached in conductive areas for samples processed at 450 °C and 500 °C, respectively.

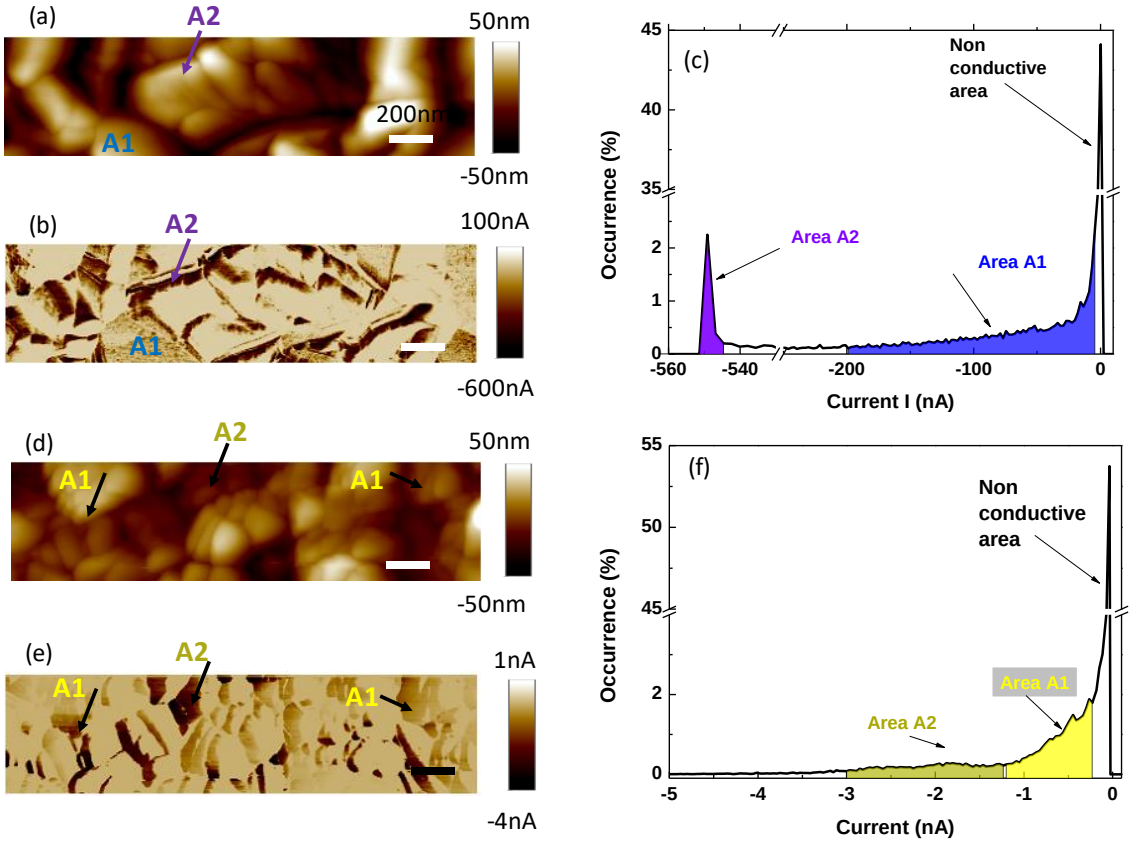

Figure 6 a Topography and **b** current maps, and **c** corresponding occurrence diagram of MOCVD films processed at 325 °C. **d** Topography and **e** current maps, and **f** corresponding occurrence diagram of MOCVD films processed at 400 °C. Current maps were obtained with bias voltage of -3 V. Scale bar corresponds to 200 nm for both AFM micrographs and red arrow correspond to conductive grain facets

With the aim to compare these films of various thickness, Fig. 7a presents the evolution of the current as a function of the electric field. The current is probed on the highest conductive areas (areas A2 on occurrence diagram on Fig. 6c and 6f). The current versus electric field characteristics have the same shape as for PECVD films. Moreover, as previously, the slope of the linear part is extracted (red dots), which reflects in first approximation the behavior of the inverse of transversal resistance. Fig. 6b represents the evolution of the inverse of slope and of the conduction area as function of Td. The transition from dense to columnar morphology, due to the increase of Td results in the increase of the transversal electrical resistance. This increase is accompanied by a decrease of the conduction area which in turn implies an increase of the transverse resistance at the microscale. The insert in Fig. 7b compares the evolution of the percentage of conductive surface and the number of different conductive areas as function of deposition temperature of MOCVD samples. These results emphasize a strong correlation

between the percentage and the number of conductive areas. Samples with only one conductive area present equally a small percentage of conductive area (less than 10% for films deposited at 350, 450 and 500 °C), despite the different morphologies, electronic band gaps and textures. Moreover, films deposited at 325 and 350 °C present the same morphology and similar band gap, whereas their nanoscale conduction behavior is different. Thus, the number of conductive areas could be related to grains crystallographic orientations. Indeed, Warren *et al.* demonstrated on α-Fe_2O_3 films [52] that different grain orientations present different conduction behavior. Our previous studies demonstrated that such TiO_2 films present a change of crystallographic orientations with increasing the temperature [26]. At 325 °C, <100> is one of the preferential growth directions, whereas at 500 °C, this is no longer the case and <110> appears to be one of the main growth directions. Both samples would also have other growth directions, with potentially higher Miller indexes. At 400 °C, the sample presents a weak, transition texture.

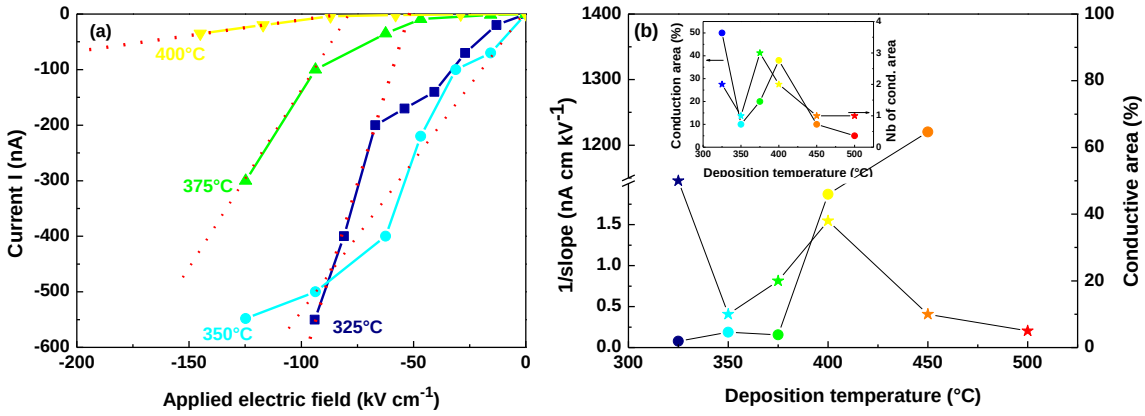

Figure 7 a C-AFM current versus applied electric field curves, probed in the highest conductive facet areas (labelled A2 on Fig. 5c and 5f) for TiO_2 films processed by MOCVD at different temperatures. Linear part of current versus electric field is depicted in red dot to extract slope. **b** Evolution of the inverse of slope and conduction area as function of deposition temperature. In insert, evolution of the amount of conduction area and the number of different conduction areas as function of deposition temperature for MOCVD TiO_2 films.

Three dimension electrical properties of TiO_2 films

Fig. 8 compares EIS spectra, represented in a Niquyst plot configuration, obtained for PECVD and MOCVD films. For all samples, only one curvature is observed, which radius decreases with increasing the doping for PEVCD (Fig. 8a) or decreasing the deposition temperature for MOCVD (Fig. 8b) films. A total equivalent circuit (Fig. 8c), taking into account the bulk, the electrolyte (two resistors in series) and the interface (the charge transfer resistance in parallel

to interface capacitance), was used [53] to extract charge transfer resistance values that are summarized in the insert of Fig. 8a and 8b. As a complement, Fig. 8d shows as a dashed line the path (named current line) used by conducting ions in the electrolyte solution and electrons in electrode materials between both counter and working electrodes, proving the crossing of the deposited films by the current line. Concerning the PECVD samples, a decrease of the charge transfer resistance is observed with the increase of the NH_3 partial pressure, by that the nitrogen amount in the film. The MOCVD samples also show a decrease in the charge transfer resistance with decreasing the deposition temperature. The charge transfer resistance is a functional property, which is difficult to clearly relate to structural properties as the relationship between charge resistance transfer and electrode properties (lateral and transversal resistivity, porosity, electronic gap…) is not straightforward [54]. Despite this limitation, expectedly, the charge transfer resistance of both MOCVD and PECVD films evolves in the same way as the microscale lateral resistivity, the electronic band gap and the porosity.

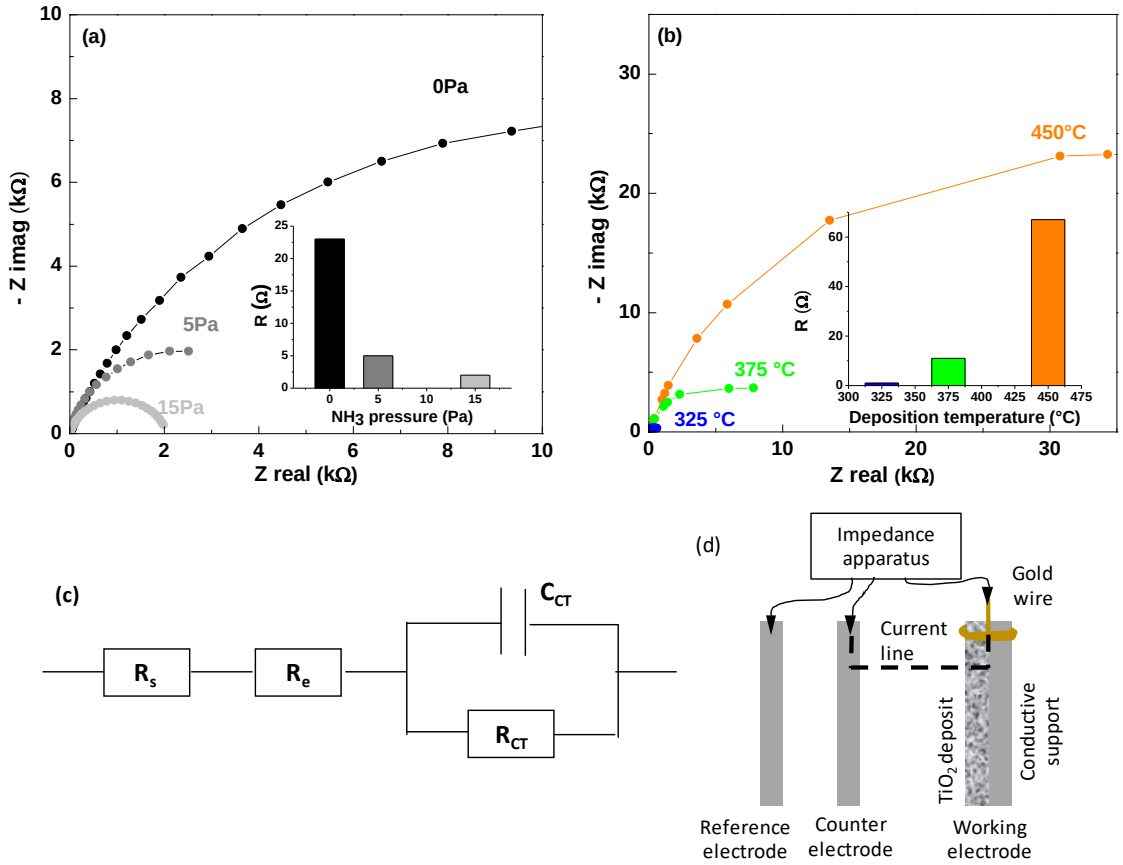

Figure 8 EIS spectra in dark configuration for **a** PECVD and **b** MOCVD TiO_2 films. In insert evolution of charge transfer resistance R determined by EIS as function of deposition conditions. **c** The total equivalent circuit used using bulk resistance (R_S), electrolyte resistance (R_e), interface capacitance (C_{CT}) and charge transfer resistance (R_{CT}). (d) EIS measurement configuration (dashed line represents the current path (named current line).

Discussion

In an attempt to compare lateral and transverse electrical properties, and to identify the influence of structural and morphological characteristics on carrier's transport, we report in Fig. 9 the mean value of the current over the probed surface and the lateral resistivity for PECVD and MOCVD TiO_2 films, respectively. C-AFM results show that for PECVD films the transversal current drastically drops when nitrogen amount increases (Fig. 9a) even if the films density simultaneously increases. This trend was observed for Sb-doped TiO_2 [17]. In the present case, morphology, current path localization through facets, dimension and amount of conductive area are quite the same for the undoped and low-doped samples, whereas there is a 20-fold decrease of the current amount for a fixed applied electric field when NH_3 pressure increases (Fig.5a). Consequently, such current decrease is related to conduction into and not between grains. This is probably due to the noticeable negative effects of impurities or disorder induced by nitrogen doping on the carrier concentration and mobility. Indeed, previous studies emphasize an increase of disorder with doping [27] with a transition from ordered to disordered columnar grains (Fig. 9b). However, the charge transfer, at the material-electrolyte interface is enhanced when the nitrogen amount increases (as shown by EIS). This highlights that the charge transfer, which is a critical electrode property for SWS application, is not only influenced by lateral and transversal resistivity in the active layer; investigation of probably crucial surface properties is out of the scope of the present study.

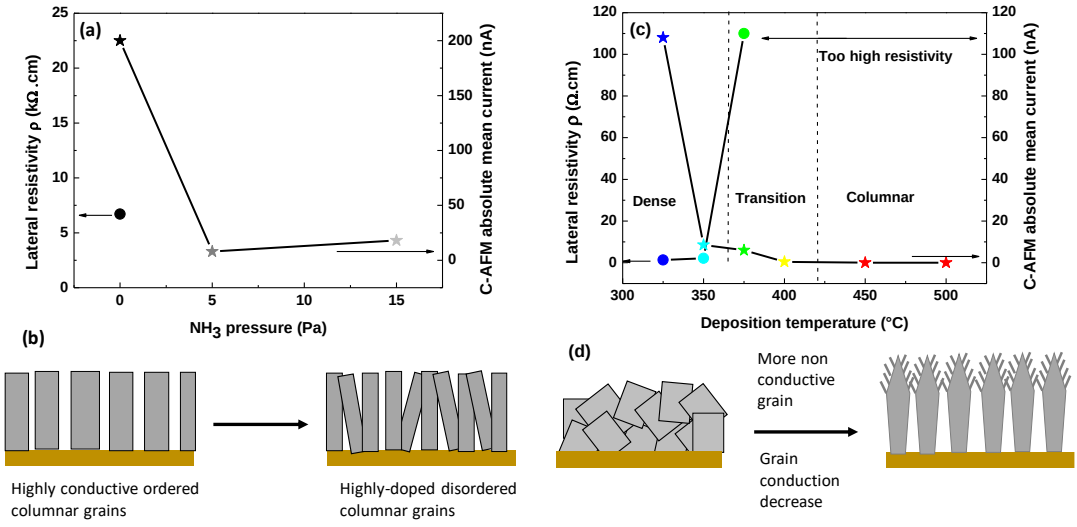

Figure 9 a Evolution of resistivity and absolute mean current for an applied electric field of 100 kV cm^{-1} as function of doping, and **b** Film morphology scheme for PECVD films. **c** Evolution of lateral resistivity and absolute mean current for an applied electric field of 100 kV cm^{-1} as function of deposition temperature, and **d** Film morphology scheme for MOCVD.

Increase of deposition temperature induces an increase of lateral resistivity and a decrease of C-AFM current in MOCVD films (Fig. 9c). This evolution is concomitant to the transition from a compact (dense) to a tree-like columnar (porous) morphology (Fig. 9d). Moreover, the decrease in the current through grains at nanoscale could be linked to the decrease of carrier mobility (table 3) and increase of the disorder [26]. According to Chen *et al* [22], such increase in lateral resistivity is linked to both the observed increase of porosity and to the decrease of the grains size, which induces an increase of the resistance through grain boundaries.

At nanoscale, undoped PECVD films with pillar-like columnar structure, and MOCVD films processed at 325 °C with dense structure, exhibit the same lateral grain size and the same current versus electric field characteristics (Fig. 5a and 7a). This indicates that the conductive grains have the same transport properties. However, the amount of conductive area is lower for MOCVD films processed at 325°C, than undoped PECVD (50 % vs 92 %). This implies that the microscale transversal resistance is higher for undoped PECVD films than in the 325 °C MOCVD films. Moreover, the latter exhibit a rather lower lateral resistivity than the undoped PECVD films, (1.3 kΩ cm vs 6.7 kΩ cm).

At the same line, MOCVD films processed at 400-500 °C and undoped PECVD films are characterized by a columnar morphology (tree-like for MOCVD [26] and pillar-like for PECVD [27]). At the nanoscale, columnar grains are less conductive and the percentage of conductive areas in MOCVD are higher than PECVD films. This imply that transversal conduction in columnar grains is some orders of magnitude lower for films processed by MOCVD at 400-500 °C than for undoped PECVD one. This could be related to lower band gap, to the different amounts of carbon [55] (chemical purity) and/or various crystallographic orientations [26-27]. Moreover, the lateral resistivity of MOCVD films is few orders of magnitude higher than PECVD ones.

Expectedly, electron transport in TiO_2 films is influenced by a complex combination of many parameters. Whatever the deposition technique is, the conduction at nanoscale decreases by the cross-linked influence of grains size decrease, disorder increase and purity decrease (i.e. doping agents which act as diffusion centers). The microscale resistivity appears inhibited by the decrease of grains resistivity and the densification of the morphology. According to this, the highest conductivity and mobility should be reached by a pure, compact, dense and ordered film with one single crystallographic orientation; this is a considerable engineering challenge for the deposition of TiO_2 films. In addition, the accurate control of C and/or N amount is crucial

to obtain pure anatase films with improved electron transport while maintaining the n-type semiconductor behavior.

Conclusions

In this paper, the relationship between film structures/morphologies and multiscale electrical was investigated. For both PECVD and MOCVD films, a strong correlation is observed between structural and electrical properties. The lateral and transversal resistivity, charge transfer resistance of MOCVD films decrease with increasing deposition temperature except for the 350°C sample. This is related to the evolution of numerous properties: the morphological transition from dense to tree-like columnar and the subsequent increase in both porosity and disorder, the texture change and the potential band gap increase. Morphology and nanoscale current of PECVD films are strongly influenced by doping. With increasing the nitrogen amount, a decrease in nanoscale current is observed, whereas the charge transfer resistance decreases. The comparison of PECVD and MOCVD films emphasizes relative contribution of morphological anisotropy and nanoscale transport along grain. The tree-like columnar structure exhibits the poor in- and out-plane conductivity properties whereas pillar-like and dense TiO_2 exhibit similar in- and out-plane conductivities even if their morphologies are really different.

Acknowledgements

This work was supported by funding from Toulouse Tech'Interlab and Association Instituts Carnot.

This project has been funded with support from Lebanese University (UL) in collaboration with AZM&SAADÉ foundation.

We are indebted to Olivier Debieu, Claire Tendero, Diane Samelor, Daniel Sadowski, Cédric Charvillat, Olivier Marsan, Jérôme Esvan, Benoît Malard, Bertrand Viguier, Alessandro Pugliara (Cirimat), Stéphane Leblond du Plouy, Arnaud Proietti, Claudie Josse (UMS Castaing) and Emmanouil Soulos (IEM) for their contributions to this work.

Compliance with ethical standards Conflict of interest

The authors declare that they have no conflict of interest

Annexes

Annex 1. TiO_2 thin films crystallographic orientation

Fig. A1 compares XRD patterns obtained in a theta-theta mode on TiO_2 films deposited by MOCVD on silicon and SiO_2 substrates respectively at the different Td. For both substrates,

peaks measured at 25.4, 38.5, 48.1, 55.1, 62.7, 70.3, 75, and 76° correspond to the (101), (112), (020), (121), (024), (220), (125), and (031) crystallographic planes of anatase, respectively. Concerning films deposited at temperature ranging from 325 °C to 400 °C on Si substrate (Fig. A1a), similar diffractograms are obtained with two major peaks (101) and (020). At higher temperature (450°C-500°C), we assist to the vanishing of (101) and (020) peaks whereas the (112) and the (220) peaks increase. The same behavior is observed for films deposited on SiO_2 substrate. These results emphasize that for our TiO_2 films the substrate has only a slight influence on films morphology.

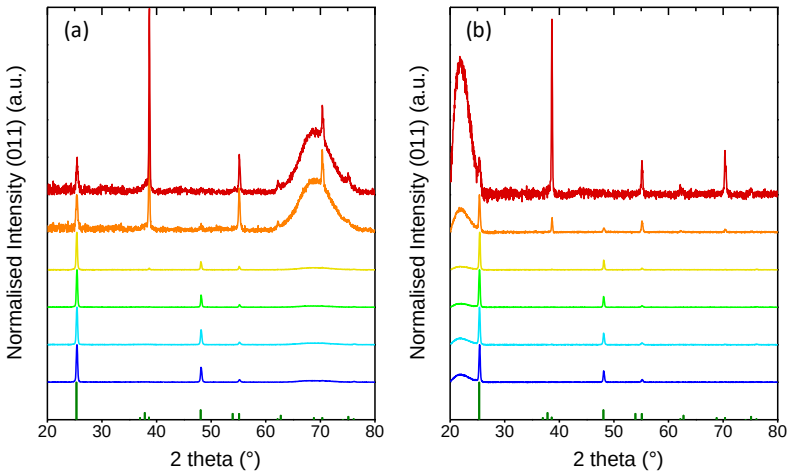

Figure A1 XRD patterns of TiO_2 films deposited by MOCVD on **a** Silicon and **b** SiO_2 substrates for various Td. The following color coding is used: 325°C (dark blue), 350°C (light blue), 375°C (green), 400°C (yellow), 450°C (orange) and 500°C (red).

Annex 2. TiO_2 absorption spectrum

Fig. A2a represents the transmission spectra for various deposition temperatures. At high temperature interference fringes are clearly visible. Interferences and increasing of transmission signal compared to low temperature are due to high surface roughness related to large structures. Figures from A2b to A2e depict the Tauc plot of the absorption coefficient α for indirect semiconductors related to transmission spectrum (Fig. A2a). The tangent plot permits to determine energy gap. However, some issues appear at low and high temperatures. For low temperature (325°C and 350°C), the gap determination is impossible as the linear part is not reached. For high temperature (450°C and 500°C), the gap determination is possible but interference fringes impact determination reliability.

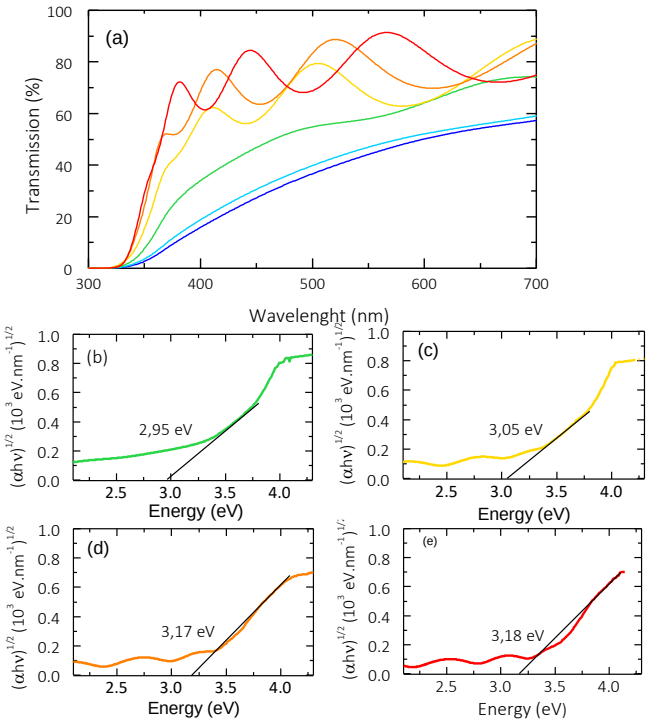

Figure A2 a Transmission spectra for TiO_2 layers processed by MOCVD at different temperatures. The following color coding is used: 325°C (dark blue), 350°C (light blue), 375°C (green), 400°C (yellow), 450°C (orange) and 500°C (red). Tauc plot of the absorption coefficient determined by UV–Vis-Nir transmission spectroscopy for samples deposited at **b** 375°C, **c** 400°C, **d** 450°C and **e** 500°C.

References

[1] Kim SK, Choi GJ, Lee SY, Seo M, Lee SW, Han JH, Ahn HS, Han S and Hwang CS (2008) Al-doped TiO_2 films with ultralow leakage currents for next generation DRAM capacitors. Adv Mat 20:1429

[2] Archa T, Arivanandhan M and Jayavel R (2019) TiO_2 nanostructures with controlled morphology for improved electrical properties of photoanodes and Quantum Dot sensitized solar cell characteristics. Surfaces and Interfaces 17:100350

[3] Fujishima A and Honda K (1972) Electrochemical Photolysis of Water at a Semiconductor Electrode. Nature 238:37-38

[4] Singh R and Dutta S (2018) A review on H_2 production through photocatalytic reactions using TiO2/TiO2-assisted catalysts. Fuel 220:607

[5] Docampo P, Guldin S, Steiner U and Snaith H J (2013) Charge Transport Limitations in Self-Assembled TiO_2 Photoanodes for Dye-Sensitized Solar Cells. J. Phys. Chem. Lett. 4:69

[6] Suhail MH, Mohan Rao G and Mohan S (1992) dc reactive magnetron sputtering of titanium-structural and optical characterization of TiO_2 films. J. Appl. Phys. 71:1421

[7] Niemelä JP, Marin G and Karppinen M (2017) Titanium dioxide thin films by atomic layer deposition: a review. Semicond. Sci. Technol. 32:093005

[8] Baryshnikova M, Filatov L, Mishin M, Uvarov A, Kondrateva A and Alexandrov S (2015) Evolution of the microstructure in titanium dioxide films during chemical vapor deposition. Phys. Status Solidi 212:1533
[9] Kim SJ, Dang VS, Xu K, Barreca D, Maccato C, Carraro G, Bhakta RK, Winter M, Becker HW, Rogalla D, Sada C, Fischer RA and Devi A (2015) MOCVD of TiO_2 thin films from a modified titanium alkoxide precursor. Phys. Status Solidi A 7:1563
[10] Amassian A, Desjardins P and Martinus L (2004) Study of TiO_2 film growth mechanisms in low-pressure plasma by in situ real-time spectroscopic ellipsometry. Thin Solids Films 447-448:40
[11] Li D, Goullet A, Carette M, Granier A and Ladesman JP (2016) Effect of growth interuptions on TiO2 films deposited by plasma enhanced chemical vapour deposition. Materials Chemistry and Physics 182:409
[12] Rafieian D, Ogieglo W, SavenijeT, and Lammertink R G H (2015)Controlled formation of anatase and rutile TiO_2 thin films by reactive magnetron sputtering. AIP Advances 5, 097168
[13] Suciu RC, Indrea E, Silipas TD, Dreve S, Rosu MC, Popescu V, Popescu G and Nascu HI (2009) TiO_2 thin films prepared by sol – gel method. J. Phys.: Conf. Ser. 182:012080
[14] Karuppuchamy S, Nonomura K, Yoshida T, Sugiura T and Minoura H (2002) Cathodic electrodeposition of oxide semiconductor thin films and their application to dye-sensitized solar cells. Solid State Ionics 151:19
[15] Tang H, Prasad K, Sanjinès R, Schmid PE and Lévy F (1994) Electrical and optical properties of TiO_2 anatase thin films. J. Appl. Phys. 75:2042
[16] Bakri AS, Sahdan MZ, Adriyanto F, Raship NA, Said NDM, Abdullah SA and Rahim MS (2017) Effect of annealling temperature of titanium dioxide thin films on structural and electrical properties. AIP Conferences Proceeding 1788:030030
[17] Lévy F, Berger H, Forro L, Zuppiroli L, Emin D and Chauvet O (2002) High mobility n - type charge carriers in large single crystals of anatase (TiO_2). J. Appl. Phys. 75:633
[18] Dorow-Gerspach D and Wuttig M (2019) Metal-like conductivity in undoped TiO_{2-x}: Understanding an unconventional transparent conducting oxide. Thin Solid Films 669:1
[19] Hun Oh S, Jin Kim D, Hong Hahn S and Jung Kim E (2003) Comparison of optical and photocatalytic properties of TiO_2 thin films prepared by electron-beam evaporation and sol-gel dip-coating. Mater. Lett. 57:4151
[20] Chen J, Tao HB, Liu B (2017) Unraveling the intrinsic structures that influence the transport of charges in TiO_2 electrodes. Adv. Energy Mater. 1700886:1–30
[21] Song SH, Wang X and Xiao P (2002) Effect of microstructural features on the electrical properties of TiO_2. Materials Science and Engineering B 94:40
[22] Bhachu DS, Egdell RG, Sankar G, Carmalt CJ and Parkin IP (2017) Electronic properties of antimony-doped anatase TiO_2 thin films preparated by aerosol assisted chemical vapour deposition. J. Mater. Chem. C 5:9694
[23] Hernadez S, Hidalgo D, Sacco A, Chiodoni A, Lamberti A, Cauda V, Tresco E and Saracco G (2015) Comparison of photocatalytic and transport properties of TiO_2 and ZnO nanostructures for solar-driven water splitting. Phys. Chem. Chem. Phys. 17:7775
[24] Almeida de Souza Filho E, Pieretti EF, Teixeira Bento R, Marina Fuser Pillis M (2020) Effect of nitrogen-doping on the surface chemistry and corrosion stability of TiO2 films. J Mater Res and Technol 9(1): 922-934
[25] A Slonopas, M Melia, K Xie, T Globus, JM Fitz-Gerald, P Norris (2016) Factors limiting doping efficiency of Iridium in pulsed laser deposited TiO2 transparent conducting oxide. J. Mat. Sci. 51:8995
[26] Miquelot A, Debieu O, Rouessac V, Villeneuve C, Prud'homme N, Cure J, Constantoudis V, Papavieros G, Roualdes S and Vahlas C (2019) TiO_2 nanotree films for the production of

green H2 by solar water splitting: From microstructural and optical characteristics to the photocathalytic properties. Applied Surface Science 494:1127
[27] Youssef L, Kinfack Leoga-infack AJ, Roualdes S, Bassil J, Zakhour M, Rouessac V, Ayral A and Nakhl M (2017) Optimization of N-doped TiO_2 multifunctional thin layers by low frequency PECVD process. European Ceramic Society 37:5289
[28] Chen J, Bin Yang H, Tao HB, Zhang L, Miao J, Wang HY, Chen J, Zhang H and Liu B (2016) Surface rutilization of anatase TiO_2 nanorods for creation of synergistically bridging and fencing electron highways. Adv. Funct. Mater. 26:456
[29] Murakami K, Rommel M, Hudec B, Rosova A, Husekova K, Dobrocka E, Rammula R, Kasikov A, Han JH, Lee W, Song SJ, Paskaleva A, Bauer AJ, Frey L, Frohlich K, Aarik J and Hwang CS (2014) Nanoscale Characterization of TiO_2 Films Grown by Atomic Layer Deposition on RuO_2 Electrodes. Appl. Mat. Interfaces 6:2486
[30] Duminica F D, Maury F and Senocq F (2004) Atmospheric pressure MOCVD of TiO_2 thin films using various reactive gas mixtures. Surf. Coat. Techn., 188, 255:259
[31] Yu YP, Liu W, Wu and Li SW (2012) Impact of Nitrogen Doping on Electrical Conduction in Anatase TiO_2 Thin Films, J. Phys. Chem. C 116, 37, 19625:19629
[32] Aviziotis IG, Cheimarios N, Duguet T, Vahlas C and Boudouvis AG (2016) Multiscale modeling and experimental analysis of chemical vapor deposited aluminum films: linking reactor operating conditions with roughness evolution. Chem. Eng. Sci. 155:449
[33] Hersee SD and Ballingall JM (1990) The operation of metalorganic bubblers at reduced pressure. Journal of Vacuum Science & Technology A 8:800
[34] Tauc J (1968) Optical properties and electronic structure of amorphous Ge and Si. Mater. Res. Bull. 3:7
[35] Gunes M, Sato H, Pinsard-Gaudart L, Berardan D and Dragoe N (2017) A versatile system for Hall effect measurements at high temperature. Meas. Sci. Technol. 28:105905
[36] Lindemuth J and Mizuta S I (2011) Hall measurements on low-mobility materials and high resistivity materials, Proc. SPIE 8110, Thin Film Solar Technology III, 81100I (https://doi.org/10.1117/12.893100)
[37] Werner F (2017) Hall measurements on low-mobility thin films, J. Appl. Phys 122, 135306
[38] https://patents.google.com/patent/US9041389B2/en
[39] Pecunia V, Occhipinti L G, Chakraborty A, Pan Y and Peng Y (2020) Lead-free halide perovskite photovoltaics: Challenges, open questions, and opportunities, APL Materials 8, 100901
[40] Youssef L, Roualdes S, Bassil J, Zakhour M, Rouessac V, Lamy C and Nakhl M (2019) Effect of plasma power on the semiconducting behavior of low-frequency PECVD TiO_2 and nitrogen-doped TiO_2 anodic thin coatings: photo-electrochemical studies in a single compartment cell for hydrogen generation by solar water splitting. J. Appl. Electrochem 49:135
[41] Asahi R, Morikawa T, Ohwaki T, Aoki K and Taga Y (2001) Visible-light photocatalysis in nitrogen-doped titanium dioxide. Science 293:269
[42] Zhao Z and Liu Q (2008) Mechanism of higher photocatalytic activity of anatase TiO_2 doped with nitrogen under visible-light irradiation from density functional theory calculation. J Phys D Appl Phys 41:025105
[43] Bak T, Nowotny J and Nowotny MK (2006) Defect Disorder of Titanium Dioxide. J. Phys. Chem. B 110:21560
[44] Nowotny J, Alim MA, Bak T, Idris MA, Ionescu M, Prince K, Sahdan MZ, Sopian K, Mat Teridie MA and Sigmundf W (2015) Defect chemistry and defect engineering of TiO_2-based semiconductors for solar energy conversion. Chem. Soc. Rev. 44:8424

[45] Bernardi M I B, Lee E J H, Lisboa-Filho P N, Leite E R, Longo E and Varela J A (2001) TiO_2 Thin Film Growth Using the MOCVD Method, Mat. Res. vol.4 no.3 São Carlos July 2001 (https://doi.org/10.1590/S1516-14392001000300014),
[46] Cheng X, Gotoh K, Nakagawa Y, and Usami N (2018) Effect of substrate type on the electrical and structural properties of TiO_2 thin films deposited by reactive DC sputtering, Journal of Crystal Growth 491, 120–125
[47] Michalas L, Khiat A, Stathopoulos S and Prodromakis T (2018) Electrical characteristics of interfacial barriers at metal—TiO_2 contacts. J. Phys. D: Appl. Phys. 51:425101
[48] Yildiz A, Lisesivdin SB, Kasap M and Mardare D (2007) High temperature variable-range hopping conductivity in undoped TiO_2 thin film. Optolectronics and advanced materials 1:531
[49] Wang W, Feng X , Ma X, He L , Cao Q and Ma J (2017) Epitaxial growth and properties of Nb-doped anatase TiO_2 films on LSAT by MOCVD, Journal of Alloys and Compounds 729, 38-42.
[50] Krasienapibal TS, Fukumura T, Hirose Y and Hasegawa T (2014) Improved room temperature electron mobility in self-buffered anatase TiO_2 epitaxial thin film grown at low temperature. Jpn. J. Appl. Phys. 53:090305
[51] Youssef L (2018) Développement par procédé plasma de couches minces de type TiO_2 dopé à l'azote pour la production d'hydrogène par photo-électrolyse de l'eau sous lumière solaire, PhD thesis, 19 novembre 2018 (Univ. Montpellier, France)
[52] Warren SC, Voitchovsky K, Dotan H, Leroy CM, Cornuz M, Stellaci F, Hebert C, Rothschild A and Grätzel M (2013) Indentifying champion nanostructures for solar water-splitting. Nature materials 12:842
[53] Sorensen PR (1982) Conductivity, charge transfer and transport number – an AC-investigation of the polymer electrolyte LiSCN-poly(ethylenoxide). Electrochimica Acta 27:1671
[54] Nara H, Mukoyama D, Shimizu R, Momma T and Osaka T (2019) Systematic analysis of interfacial resistance between cathode layer and the current collector in lithium-ion batteries by electrochemical impedance spectroscopy. J. Power Sources 409:139
[55] Nizard H, Kosinova ML, Fainer NI, Rumyantsev YM, Ayupov BM and Shubin YV (2008) Deposition of titanium dioxide from TTIP by plasma enhanced and remote plasma enhanced chemical vapor deposition. Surface and Coating Technology 202:4076